IEEE Access
Multidisciplinary | Rapid Review | Open Access Journal

Received April 8, 2019, accepted May 23, 2019, date of publication May 30, 2019, date of current version June 17, 2019.

Digital Object Identifier 10.1109/ACCESS.2019.2920015

Ramp Distribution-Based Contrast Enhancement Techniques and Over-Contrast Measure

SEUNGYOUN LEE[1] AND CHANGICK KIM[2], (Senior Member, IEEE)
[1]Agency for Defense Development, Daejeon 34060, South Korea
[2]Department of Electrical Engineering, Korea Advanced Institute of Science and Technology, Daejeon 34141, South Korea

Corresponding author: Changick Kim (changick@kaist.ac.kr)

ABSTRACT Our approach to contrast enhancement (CE) of images is based on natural scene statistics (NSS). We show, in this paper, that the average intensity distribution of natural images can be linearly approximated to the ramp distribution in an ordered histogram domain as the contrast increases. Based on this finding, we propose ramp distribution-based global and local CE algorithms. The ramp distribution-based slant thresholding (RDST) algorithm is proposed as a global CE method which uses slant thresholding in an ordered histogram domain to yield a contrast-enhanced image. Also, the ramp distribution-based adaptive slant thresholding (RDAST) algorithm is proposed as a local CE method. It adaptively adjusts a slant angle of the ramp distribution in each block to suppress noise amplification in uniform regions and maximizes contrast in non-uniform regions. The RDAST also employs a scaled global modified histogram to minimize sensitivity to block size changes. Moreover, we propose a metric to measure the amount of over-contrast in an image to evaluate all CE algorithms more correctly. The experimental results show that the proposed algorithms have better or competitive performance as well as computational efficiency.

INDEX TERMS Image enhancement, contrast enhancement, ramp distribution, over-contrast measure.

I. INTRODUCTION

Thanks to the proliferation of digital imaging devices such as cameras and smartphones, taking and sharing photos have become a daily routine. According to people's desire to get high-quality images and vendors' effort to provide a high quality of experience, a number of image-enhancing techniques have been actively studied. Considering the fact that contrast is an important factor in the human perception of image quality, applying the contrast enhancement (CE) method is one of the most effective ways to enhance images.

Improving the contrast not only makes the image more visually pleasing but also helps us to understand the contents of the image. For example, it can make us distinguish interesting objects from improved backgrounds. Besides, CE is often adopted as a pre-processing step for many computer vision problems including object recognition [1], [2], object-of-interest image segmentation [3], [4] medical images enhancement to detect and interpret diseases [5], [6].

The associate editor coordinating the review of this manuscript and approving it for publication was Po Yang.

A. MOTIVATION

Natural scene statistics (NSS) models have been developed based on the hypothesis that natural images possess certain regular statistical properties, and they have proven to be powerful tools driving various image/computer vision applications [7]. To our best knowledge, however, to date no effort has been applied towards modeling NSS for CE. We propose to use the the ramp distribution as a model of NSS for improving contrast. Intuitively, this is the distribution that increases with a constant slant angle defined in the ordered histogram domain as shown in Fig. 1(a).

We carried out NSS using the SUN database [8] containing 108,754 images. The normalized input histograms, i.e., probability distribution function (PDF), of all images in the database are transformed into the ordered histogram domain by sorting non-zero gray-levels according to its frequency. To calculate averages of sorted PDFs, the dynamic range of the ordered histogram domain is adjusted to have the entire dynamic range of the input image using a bi-linear interpolation method. Results of averages of sorted PDFs according to quantized contrast amounts are shown in Fig. 1(a), where the contrast amounts of images are

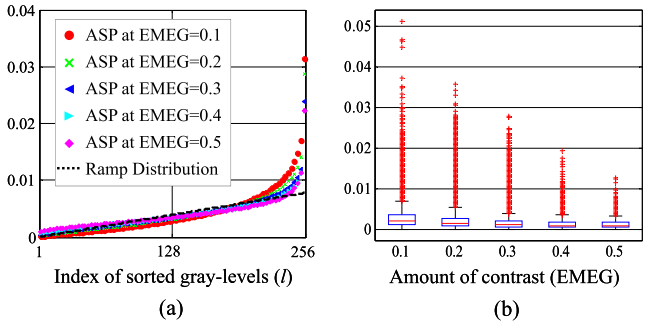

FIGURE 1. The ramp distribution in natural scene statistics. (a) Averages of sorted PDFs (ASP) according to contrast amounts (EMEG) and the ramp distribution. (b) A boxplot of RMSE values[1] according to EMEG values.

measured by using the expected measure of enhancement by gradient (EMEG) [20]. Figure 1(b) shows a boxplot of the root-mean-square-errors (RMSE) values[1] according to EMEG, where the RMSE values are calculated between sorted PDFs and the ramp distribution. We demonstrate that the average distribution of the natural images in the ordered histogram domain can be linearly approximated to the ramp distribution as contrast increases as shown in Fig. 1(a). It is more evidently observed in Fig. 1(b) that the more the contrast amount, the smaller the values of RMSE. It means that the contrast-enhanced images as a result of CE methods should be close to the ramp distribution in the ordered histogram domain to follow NSS. By doing this, it is possible to produce contrast-improved images while maintaining naturalness. This finding motivates us to employ the ramp distribution for CE.

B. CONTRIBUTIONS

- A new global CE algorithm of ramp distribution-based slant thresholding (RDST) is proposed. It employs the new threshold strategy of *slant thresholding*, which automatically determines threshold values in an ordered histogram domain. The differences between the conventional and the proposed thresholding technique are discussed.
- Further, a new local CE algorithm of ramp distribution-based adaptive slant thresholding (RDAST) is proposed. Conventional local CE methods often produce excessively amplified noise in uniform regions and are sensitive to block size settings resulting in blocking artifacts. To address these issues, the RDAST automatically controls the levels of CE for each block by adjusting a slant angle of the ramp distribution and utilizes a scaled global histogram to minimize the effect to block size changes.
- We have investigated the limitation of image quality assessment (IQA) metrics for contrast-changed images in the viewpoint of the overshoot effect. As a result, we have found that even state-of-the-art IQA metrics for contrast-changed images cannot correctly evaluate the overly contrasted images. To deal with this problem, we propose an over-contrast measure (OCM) to quantify the amount of over-contrast in an image. It measures amplified detail amounts in the uniform regions by using the guided filter. The proposed OCM helps us to evaluate the quality of contrast-changed images more accurately.

The rest of this paper is organized as follows. Literature survey on related work is presented in Section II. Section III describes the proposed CE algorithms. Section IV shows the proposed over-contrast measure, and Section V presents quantitative and qualitative comparisons of the proposed algorithms with state-of-the-art CE algorithms. Finally, concluding remarks are given in Section VI.

II. RELATED WORK

CE techniques can be categorized into two groups: direct methods and indirect methods [12]. We focus on indirect methods which improve the contrast by redistributing the intensities to utilize the whole dynamic range effectively. Numerous indirect CE techniques have been proposed [9]–[25]. It can be subdivided into global CE and local CE methods.

A. GLOBAL CONTRAST ENHANCEMENT

Histogram equalization (HE) [9] is the most fundamental CE method due to its simplicity and quickness. HE finds a mapping function between input gray-levels to output gray-levels by calculating cumulative distribution function (CDF) from an input histogram. However, HE often produces an over-enhanced (or under-enhanced) image especially when there are large peaks in the input histogram which usually correspond to homogeneous regions, resulting in a noisy and washed-out appearance of the enhanced image. To solve this problem, the following algorithms [10]–[22] have been proposed.

1) HISTOGRAM MODIFICATION

Weighting and thresholding histogram equalization (WTHE) [10] clamps an input PDF at an upper and a lower threshold. Then, it weights all values between the thresholds using a normalized power-law function with power index γ which is a critical parameter controlling the degree of image enhancement. Its performance is highly dependent on the values of the parameters. Adaptive gamma correction with weighting distribution (AGCWD) [11] is proposed based on gamma correction [9]. It attempts to replace the fixed parameter γ to adaptive gamma correction calculated from CDF, i.e., γ = 1-CDF. However, AGCWD does not fully exploit the whole dynamic range of the output image. It also often produces the image that is too bright with loss of details. A histogram modification framework (HMF) [12] is proposed to use the modified histogram which is a weighted average of an input histogram $\mathbf{H}_x$ and a uniformly distributed histogram $\mathbf{H}_u$, i.e., $\mathbf{H}_m = (\mathbf{H}_x + \lambda\mathbf{H}_u)/(1+\lambda)$. In this way, an intermediate image is produced between the input image

[1] A value of RMSE = $\sqrt{\frac{1}{L}\sum_{l=1}^{L}\left(\frac{h_s(l)-h_r(l)}{HW}\right)^2}$. Detailed notations are presented in Section III-B.

and the resulting image of HE. This method somewhat compensates for the shortcomings of the HE method. However, it cannot always guarantee image quality and artifact prevention. Inspired by HMF, we proposed a ramp distribution based histogram modification (RDHM) method [13] for infrared images, where the ramp-distributed histogram is incorporated into an optimization problem with a sorted histogram of the input image to calculate a modified histogram. Although this method may result in an improvement in perceived contrast, it requires appropriate parameter settings.

2) IQA METRIC BASED AUTOMATIC PARAMETERS TUNING

Robust image contrast enhancement (RICE) [14] combines $\mathbf{H}_x$ with its equalized histogram $\mathbf{H}_{eq}$, and its sigmoid transferred histogram $\mathbf{H}_{sig}$ to calculate $\mathbf{H}_m$, i.e., $\mathbf{H}_m = (\mathbf{H}_x + \phi\mathbf{H}_{eq} + \psi\mathbf{H}_{sig})/(1 + \phi + \psi)$. ROHIM[2] [15] creates an output image using the transfer mapping which combines mean-shifting and logistic functions. Recently proposed BOIEM[3] [16] is designed based on a cascade combination of AGCWD and RICE. The parameters of these algorithms are determined by each dedicated quality assessment metric. These methods sometimes do not produce well-improved images. Besides, ROHIM and BOIEM take a long time to execute with large standard deviations.

3) 2D HISTOGRAM-BASED TECHNIQUES

CE methods using a two dimensional (2D) histogram have been developed [17]–[19] to enhance local details by increasing the gray-level differences between neighboring pixels. Recently, a method of combining two histograms (COTH) was developed to preserve both the shape of a 1D histogram and the statistical information of a 2D histogram. Compared to using the only 1D histogram, 2D histogram-based methods typically produce output with less visual distortions. However, constructing a 2D histogram is computationally expensive, and the complexity increases exponentially as the size of adjacent regions increases.

4) SPATIAL 2D HISTOGRAM-BASED TECHNIQUES

Unlike the 1D or 2D histogram-based methods, the distribution of spatial locations of gray-levels of an image is considered in [20]–[22]. Spatial entropy based CE (SECE) [20] method uses a spatial entropy in a 2D spatial histogram. Residual SECE [21] considers the spatial joint relationships of gray-levels by introducing residual spatial entropy. Recently, spatial mutual information and PageRank-based CE (SMIR) [22] is proposed to use the rank vector of gray-levels resulted from PageRank algorithm where gray-levels are used to represent nodes in PageRank, and the weights between nodes are computed according to spatial mutual information. Although the performance of the SMIR is satisfactory, it requires a lot of memory and its calculation time is irregular.

[2]ROHIM is an acronym for a Reduced-reference image quality metric for contrast change based Optimal HIstogram Mapping.

[3]BOIEM is an acronym for a Blind image quality measure of enhanced images based Optimized Image Enhancement Method.

B. LOCAL CONTRAST ENHANCEMENT

The main disadvantage of global CE methods is that global histogram information may not appropriately enhance some parts of the image since it treats all regions of the image equally. Therefore, local CE methods have been proposed. Adaptive histogram equalization (AHE) [23] uses a small rectangular block that slides sequentially over all pixels in the input image, and the histogram of pixels within the current position of the block is equalized. Contrast-limited AHE (CLAHE) proposed [24] to address two main problems of AHE: calculation time and over-enhancement. To reduce calculation time, it divides the input image into equally-sized blocks. The output image is obtained by applying bilinear interpolation between processed blocks to remove possible blocking artifacts. To address the over-enhancement problem, it limits the peak value in the histogram of each block by clipping the histogram at a predefined value. The clipped pixels are redistributed to limit the slope of the CDF. The performance of CLAHE is determined by the block size and the clip-limit which are typically selected by users. Recently, dual gamma correction based CLAHE [25] has been proposed for dark image enhancement. This method has many parameters that need to be set in advance, and the performance of the algorithm also depends on the values of the parameters.

III. PROPOSED ALGORITHMS

A. PROBLEM DEFINITION

Let $\mathbf{X} = \{\mathbf{X}(i,j)|1 \le i \le H, 1 \le j \le W\}$ be an gray-scale input image with size of $H \times W$ pixels, where $\mathbf{X}(i,j)$ is a gray-level (intensity) x_k of a pixel location (i,j), and $\mathbf{X}(i,j) \in [x_1, x_K], \forall(i,j)$. Let $\mathcal{X} = \{x_1, x_2, \ldots, x_K\}$ be the sorted set of all possible K gray-levels that exist in an input image $\mathbf{X}$ where $x_1 < x_2 < \ldots < x_K$, K is the number of distinct gray-levels. Let $\mathbf{Y} = \{\mathbf{Y}(i,j)|1 \le i \le H, 1 \le j \le W\}$ be the output image and $\mathcal{Y}$ be a sorted list of output gray-levels $\mathcal{Y} = \{y_1, y_2, \ldots, y_K\}$ where $y_1 \le y_2 \le \ldots \le y_K$, and $\mathbf{Y}(i,j) \in [y_1, y_K], \forall(i,j)$. The goal of the CE algorithm is to produce the output image $\mathbf{Y}$ that not only has improved contrast but also looks natural. The output image can be obtained as $\mathbf{Y} = f(\mathbf{X}) = \{f(\mathbf{X}(i,j)) \mid \forall\mathbf{X}(i,j) \in \mathbf{X}\}$, where $f(\cdot)$ is a mapping function between $\mathcal{X}$ and $\mathcal{Y}$.

B. GLOBAL APPROACH

The histogram of an input image $\mathbf{X}$ is calculated as $\mathbf{H}_x = \{h_x(k)|1 \le k \le K\}$, where $h_x(k)$ is the number of occurrences of the kth gray-level x_k. To deal with over-enhancement of noise in homogeneous regions, a traditional approach of Plateau HE [26] calculates a modified histogram $\mathbf{H}_m = \{h_m(k)|1 \le k \le K\}$ as follows:

$$h_m(k) = \begin{cases} \mathcal{T}, & \text{if } h_x(k) > \mathcal{T}, \\ h_x(k), & \text{otherwise}, \end{cases} \tag{1}$$

where $\mathcal{T}$ is a threshold value. It is difficult to determine $\mathcal{T}$ because all images have different shapes of $\mathbf{H}_x$. Moreover, Plateau HE cannot improve the contrast effectively since it applies the same threshold value to the input histogram. To obtain effectively contrast-enhanced images, it should be considered in the thresholding process that a gray-level belonging to a high frequency of occurrence should have a higher threshold than the lower ones. It can be achieved by introducing the ramp-distributed histogram $\mathbf{H}_r$.

Let $\mathbf{H}_s = \{h_s(l)|1 \le l \le L\}$ be the sorted set of all non-zero $h_x(k)$ in ascending order, where $h_s(l)$ is an lth element of the sorted set and L is the total number of all non-zero $h_x(k)$. Let $\mathbf{H}_r = \{h_r(l)|1 \le l \le L\}$ be defined as the ramp-distributed histogram that increases with a constant slant angle, where $\sum_{l=1}^{L} h_r(l) = HW$ and $h_r(l)$ is computed as [4]

$$h_r(l) = \frac{2HW}{L(L+1)}l. \tag{2}$$

Then, the target histogram can be calculated as

$$h_t(l) = \begin{cases} h_r(l), & \text{if } h_s(l) > h_r(l), \\ h_s(l), & \text{otherwise.} \end{cases} \tag{3}$$

We call this thresholding process as *slant thresholding*. The modified histogram $\mathbf{H}_m$ is calculated according to

$$h_m(k) = h_t\left\{\Psi(l)\right\}, \tag{4}$$

where $\Psi(\cdot)$ is a function of index mapping between l and k obtained from the sorting process. The modified histogram $\mathbf{H}_m$ is normalized to give the PDF as

$$pdf(k) = h_m(k) \Big/ \sum_{k=1}^{K} h_m(k), \tag{5}$$

and the CDF is defined as

$$cdf(k) = \sum_{k=1}^{K} pdf(k). \tag{6}$$

Using the CDF, x_k is mapped to y_k according to

$$y_k = \lfloor cdf(k)(2^8 - 1) + 0.5 \rfloor. \tag{7}$$

Figure 2 illustrates the proposed ramp distribution-based slant thresholding (RDST) algorithm. A visible light image from dataset [30] is shown in Fig. 2(a) and its histogram $\mathbf{H}_x$ in Fig. 2(b). $\mathbf{H}_s$ is the sorted histogram of the non-zero gray-levels in $\mathbf{H}_x$ in ascending order as shown in Fig. 2(d). The target histogram $\mathbf{H}_t$ is acquired by using *slant thresholding* as shown in Fig. 2(d) and the resultant modified histogram $\mathbf{H}_m$ is shown in Fig. 2(b). The mapping function for the RDST algorithm is presented in Fig. 2(f). For comparison, we draw the mapping function of HE and its result image in Fig. 2(f) and (c) respectively. The output image of HE has significantly increased noise in uniform regions. On the other hand, the proposed RDST not only produces a contrast-enhanced image having a natural appearance but also effectively suppresses noise amplification in uniform regions compared to HE.

[4]The proof of Eq. (2) is presented in Appendix.

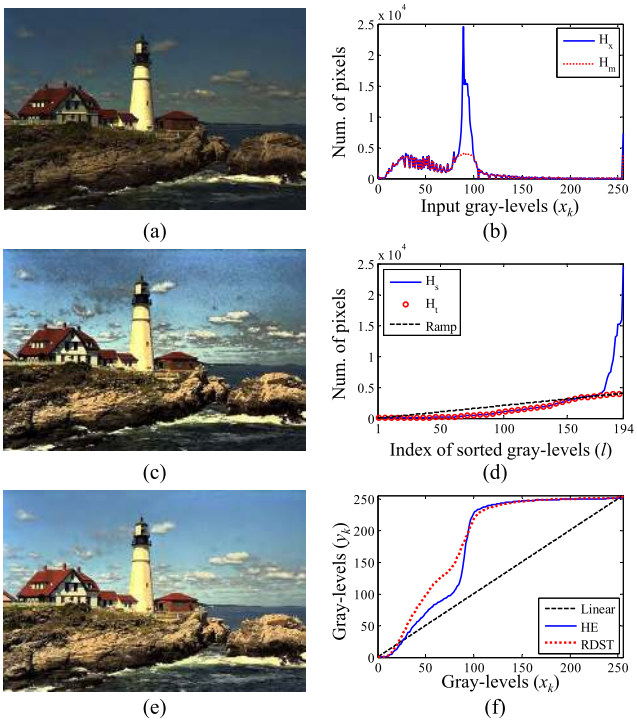

FIGURE 2. Illustrations of the proposed RDST algorithm. (a) The input image from [30]. (b) An input histogram $\mathbf{H}_x$ and a modified histogram $\mathbf{H}_m$. (c) A result of HE. (d) A sorted histogram $\mathbf{H}_s$, a target histogram $\mathbf{H}_t$, and the ramp-distributed histogram. (e) A result of RDST. (f) Corresponding mapping functions.

C. LOCAL APPROACH

1) PROPOSED LOCAL ALGORITHM

The flowchart of the proposed ramp distribution-based adaptive slant thresholding (RDAST) is presented in Fig. 3. The details of the procedure are as follows.

First, the input image $\mathbf{X}$ is divided into $M \times N$ non-overlapping blocks. A b^{th} block can be denoted as $\mathbf{X}^b = \left\{\mathbf{X}^b(m,n)|1 \le m \le M, 1 \le n \le N\right\}$, where $b \in [1, B]$ and B is the total number of blocks.

Second, let $\mathbf{h}_x^b = \{h_x^b(k)|1 \le k \le K\}$ be defined as a local histogram of the gray-level x_k in a b^{th} block. Let $\mathbf{h}_s^b = \left\{h_s^b(l)|1 \le l \le L\right\}$ be the sorted set of all possible $h_x^b(k)$ in ascending order, where $h_s^b(l)$ is an element of the sorted set of the b^{th} block and we set L to K. Note that we use all possible gray-levels in local processing by setting L to K rather than the total number of all non-zero $\mathbf{h}_x^b$ to prevent over-enhancement. Let $\mathbf{h}_r^b = \left\{h_r^b(l)|1 \le l \le L\right\}$ be defined as an adjusted ramp-distributed histogram, where

$$h_r^b(l) = \alpha \frac{2MN}{L(L+1)}l. \tag{8}$$

α is a parameter for adjusting the slant angle. For blocks in uniform regions, it is desirable to set α to a low value to avoid excessive enhancement. On the other hand, it is better to set α to a higher value for blocks in non-uniform regions so that the texture and details can be effectively enhanced. Therefore, it is necessary to adjust α adaptively according to the

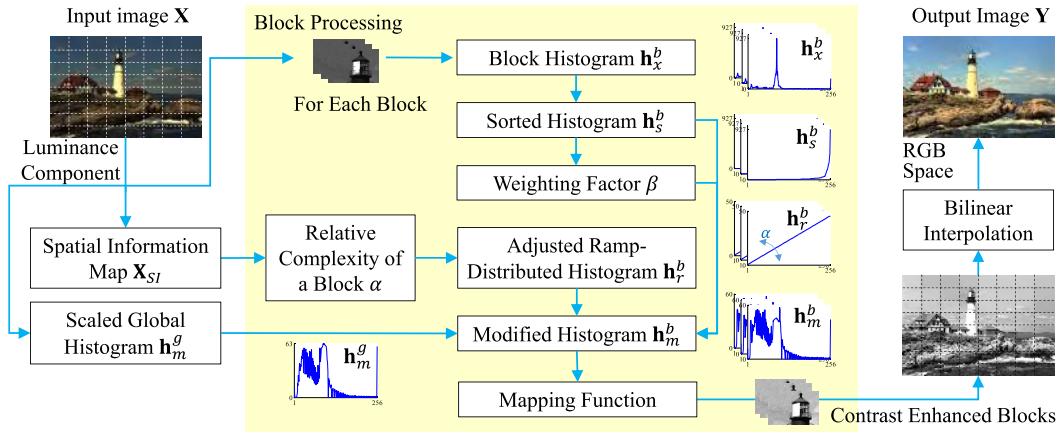

FIGURE 3. Flowchart of the proposed RDAST algorithm.

complexity of each block. To measure the complexity of a block, we employed spatial information which has been commonly used as the basis for estimating image complexity [40]. The ratio of the block's complexity with respect to the overall image complexity is used to calculate α as follows

$$\alpha = \frac{\frac{1}{MN}\sum_{m=1}^{M}\sum_{n=1}^{N}\mathbf{X}_{SI}^{b}(m,n)}{\frac{1}{HW}\sum_{i=1}^{H}\sum_{j=1}^{W}\mathbf{X}_{SI}(i,j)}, \tag{9}$$

where $\mathbf{X}_{SI}$ is a spatial information map calculated as

$$\mathbf{X}_{SI}(i,j) = \left(\mathbf{X}_x^2(i,j) + \mathbf{X}_y^2(i,j)\right)^{\frac{1}{2}}. \tag{10}$$

$\mathbf{X}_x$ and $\mathbf{X}_y$ denote gray-scale images filtered with horizontal and vertical Sobel kernels, respectively. According to the level of the complexity of input blocks, the parameter α automatically adjusts the slant angle of the ramp distribution in each block as shown in Fig. 4(c1)-(c3). As a result, details are significantly improved in the blocks of the non-uniform regions as shown in Fig. 4(d1). It becomes clearer when compared to the results of RDST as shown in Fig. 4(e1). Moreover, noise amplification is effectively suppressed in the block of the uniform regions as shown in Fig. 4(d3).

Third, the local modified histogram $\mathbf{h}_m^b = \{h_m^b(k)|1 \le k \le K\}$ can be calculated as

$$h_m^b(\psi(l)) = \begin{cases} h_r^b(l), & \text{if } h_s^b(l) > h_r^b(l), \\ (1-\beta)h_m^g(\psi(l)) + \beta h_s^b(l), & \text{otherwise,} \end{cases} \tag{11}$$

where $\psi(\cdot)$ is a function of index mapping between l and k obtained from a sorting process of a local histogram $h_x^b(k)$. $\mathbf{h}_m^g$ is a scaled global histogram calculated as

$$h_m^g(k) = h_m(k) \times (MN/HW). \tag{12}$$

β is a weighting factor between $\mathbf{h}_m^g$ and $\mathbf{h}_s^b$. We set β equals to the ratio of the area occupied by the sorted histogram in the area of a right triangle with the base of $L+1$ and the height of $h_s^b(L)$ as

$$\hat{\beta} = \frac{\sum_{l=1}^{L} h_s^b(l)}{\sum_{l=1}^{L} l\left(h_s^b(L)/L\right)} = \frac{MN}{\frac{1}{2}(L+1)h_s^b(L)}, \tag{13}$$

and $\beta = min(\hat{\beta}, 1)$. Note that the maximum value of β is limited to 1 to prevent underflow when calculating $\mathbf{h}_m^b$ in (11).

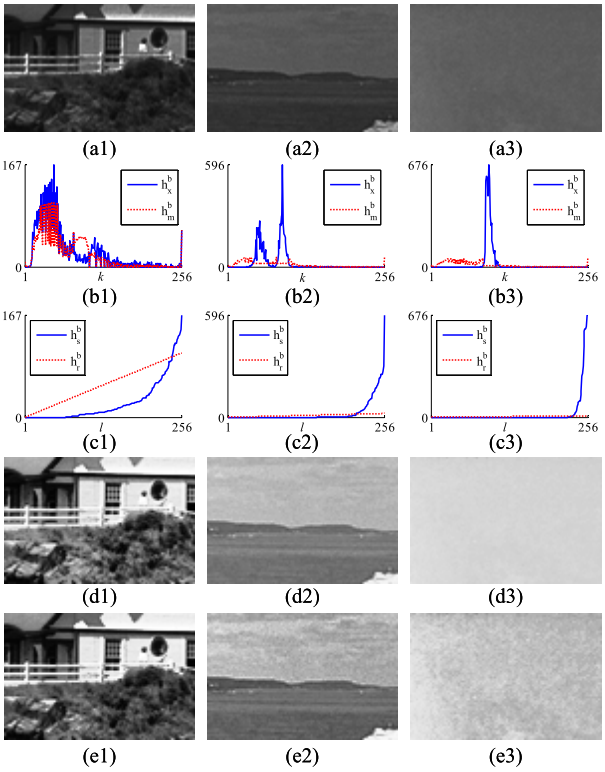

FIGURE 4. Comparisons of three sample blocks and corresponding histograms. (a1)-(a3) Sample blocks. (b1)-(b3) Corresponding input histograms $\mathbf{h}_x^b$ and modified histograms $\mathbf{h}_m^b$. (c1)-(c3) Corresponding sorted histograms $\mathbf{h}_s^b$ and adjusted ramp-distributed histograms $\mathbf{h}_r^b$. (d1)-(d3) Corresponding results of RDAST. (e1)-(e3) Corresponding results of RDST for comparisons.

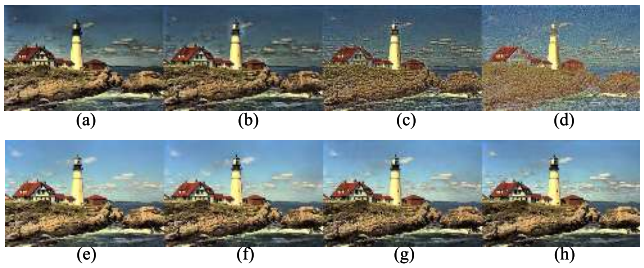

FIGURE 5. Effect of block size on CLAHE and RDAST. (a)-(d) CLAHE results according to the different block sizes of 128×128, 32×32, 8×8, and 2×2 respectively. (e)-(h) RDAST results according to the different block sizes of 128×128, 32×32, 8×8, and 2×2 respectively.

As the uniformity of the block increases, the histogram distribution becomes narrower and higher as shown in Fig. 4(b1)-(b3). As a result, the value of β is decreased, and a higher weight is assigned to $\mathbf{h}_m^g$. Therefore, the gray-levels of the block in uniform regions are determined by considering the distribution of global gray-levels. In this way, it is possible to minimize sensitivity to block size changes and prevent blocking artifacts.

Next, contrast-enhanced blocks can be obtained by applying (5)-(7) to each block by using $\mathbf{h}_m^b$. Finally, output image $\mathbf{Y}$ is obtained by applying bilinear interpolation between contrast-enhanced blocks to remove possible blocking artifacts. Refer to [24] for further information regarding bi-linear interpolation.

2) PARAMETER ANALYSIS OF RDAST

The parameters used in RDAST are designed to be automatically adjusted, so no parameters are required for manual adjustment except the block size. The performance of the existing local CE methods depends on the block size because only local histogram information is used to determine the gray-levels of each block. Therefore, the smaller the block size, the greater the blocking artifacts and distortion. However, to minimize sensitivity to block size changes, the RDAST utilizes the scaled global histogram $\mathbf{h}_m^g$ to determine the gray-levels of each modified block histogram $\mathbf{h}_m^b$. For example, Fig. 5 shows the results of CLAHE and RDAST according to the different block sizes. CLAHE generated unrealistic images as the block size decreased. On the other hand, RDAST produced reasonably consistent quality images.

IV. OVER-CONTRAST MEASURE

A. LIMITATIONS OF METRICS FOR CONTRAST-CHANGED IMAGES

Evaluating the perceptual quality of an image is a fundamental problem, and various metrics have been proposed for image quality assessment (IQA). However, it has been reported that these metrics have the overshoot effect, content dependency, and the range effect, so they have limitations in evaluating image quality correctly [36], [37]. We have investigated IQA metrics for contrast-changed images in the viewpoint of the overshoot effect, which is more closely related to the major limitation of the metrics' performance.

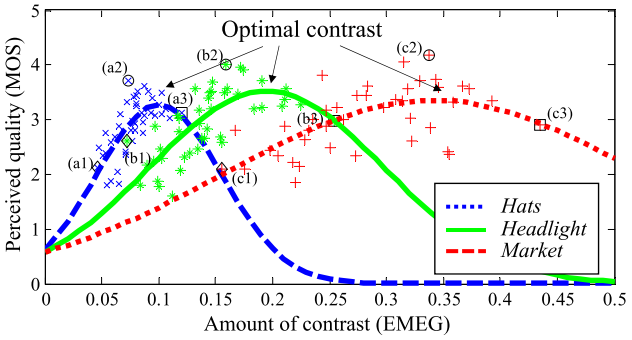

FIGURE 6. Amount of contrast (EMEG) versus perceived qualities (MOS) of three sample images. Each parenthesis indicates a sub-figure in Fig 8. For example, (a1) indicates Fig. 8(a1).

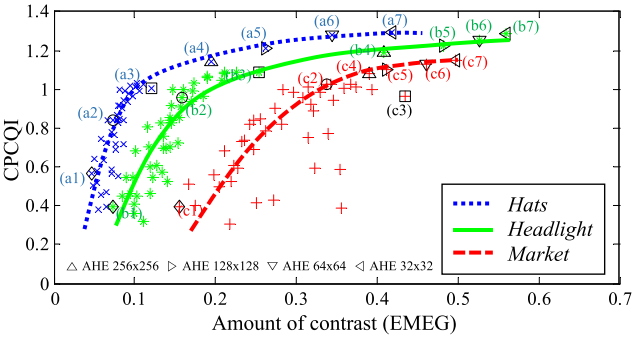

FIGURE 7. Amount of contrast (EMEG) versus CPCQI values of three sample images. Each parenthesis indicates a sub-figure in Fig 8. For example, (a1) indicates Fig. 8(a1).

The overshoot effect means that the quality of a processed image increases according to strength (e.g., sharpening amount), but after reaching the optimal point, the quality starts dropping [36]. The CCID2014 dataset [30] which was constructed to develop IQA metrics of contrast-changed images was chosen to investigate the problem. Throughout many experiments, we found that the overshoot effect is more correlated with EMEG [20] (refer to Section V-B.3 for details about EMEG) rather than other contrast measures such as root mean square contrast (RMSC) [41], a measure of enhancement (EME) and its variants [32]. The overshoot effect is observed in all images of CCID2014. For example, the changes of perceived qualities, i.e., mean opinion scores (MOS), versus the amount of contrast (EMEG) for three images, are shown in Fig. 6, where the points of optimal contrast are marked. Figure 7 shows the CPCQI values according to EMEG. To clearly see the limitation of the performance of IQA metrics, we added overly contrasted images obtained by setting the AHE algorithm to have different block sizes: 256×256, 128×128, 64×64, and 32×32 as shown in Fig. 8. Unlike the perceived qualities, the CPCQI values increase consistently as the EMEG values increase even in overly contrasted images as shown in Fig. 7. For example, the CPCQI value of 1.19 in Fig. 8(b4) is higher than the value of 0.95

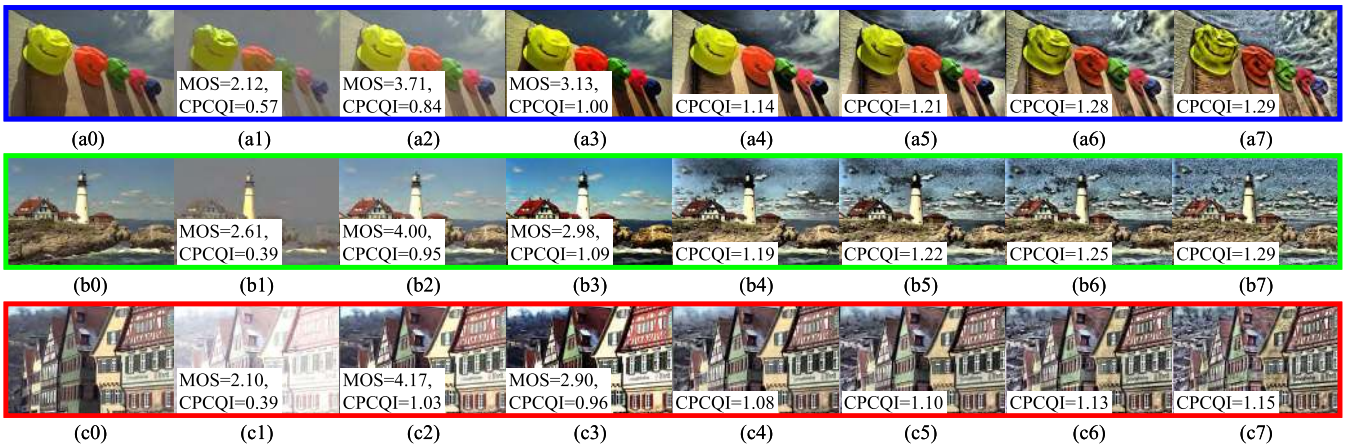

FIGURE 8. Pristine images and its contrast-changed images of *Hats*, *Headlight*, and *Market* (from top to bottom). (a0)-(c0): Pristine images. (a1)-(c1), (a2)-(c2), and (a3)-(c3) represent contrast-changed images in CCID2014 dataset [30]. (a4)-(c4) represent resulting images of AHE with block size of 256×256, (a5)-(c5) 128×128, (a6)-(c6) 64×64, and (a7)-(c7) 32×32. Available values of MOS and CPCQI are marked.

in Fig. 8(b2). The same phenomenon has been observed in other metrics including QRCM. It means that even the latest metrics do not correctly evaluate the overly contrasted images. (Refer to Section V-B for details about QRCM and CPCQI).

B. PROPOSED OVER-CONTRAST MEASURE

Due to the limitation mentioned above, the IQA metrics for contrast-changed images do not correctly evaluate the results of local CE algorithms which often produce overly contrasted images. Therefore, it is urgently required to measure the amount of over-contrast to evaluate the overly contrasted images correctly. Overly contrasted regions in an image can be seen more apparently in uniform regions than in non-uniform regions. For example, an overly contrasted image is shown in Fig. 8(b4), where the amplified noise in the sky which corresponds to uniform regions in its pristine image is apparently visible, while the over-enhancement in non-uniform regions such as rocks and houses is not noticeable. Therefore, we measure the amount of over-contrast only in uniform regions. The flowchart of the proposed over-contrast measure (OCM) is shown in Fig. 9.

1) UNIFORM REGIONS DETECTION

To detect uniform regions in an original image, we used the local standard deviation map $\mathbf{X}_\sigma$, calculated as follows

$$\mathbf{X}_\sigma = f_{\text{std}}(\mathbf{X}_{lp}) = f_{\text{std}}(\mathbf{X} * \mathbf{w}), \tag{14}$$

where $f_{\text{std}}(\cdot)$ is a local standard deviation filter which moves pixel-by-pixel over the entire image. At each step, the local standard deviation is calculated within a local 5×5 square window. To reduce noise sensitivity, we used a lowpass filtered image $\mathbf{X}_{lp}$ which is calculated by convolving an original image $\mathbf{X}$ with $\mathbf{w}$. $\mathbf{w} = \{w_i | i = 1, 2, \cdots, N\}$ is an 11×11 circular-symmetric Gaussian weighting kernel, with standard deviation of 1.5, normalized to unit sum,

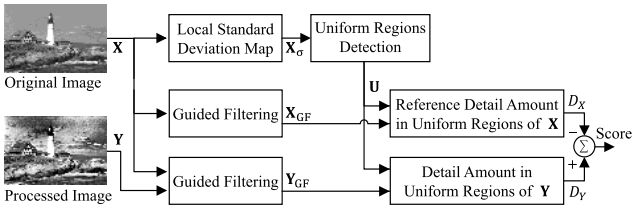

FIGURE 9. The flowchart of the proposed over-contrast measure.

i.e., $\sum_{i=1}^{N} w_i = 1$. A map of uniform region $\mathbf{U}$ is calculated as

$$\mathbf{U}(i,j) = \begin{cases} 1, & \text{if } \mathbf{X}_\sigma(i,j) \le \mathcal{T}_U, \\ 0, & \text{otherwise,} \end{cases} \tag{15}$$

where $\mathcal{T}_U$ is a threshold value. By using a standard deviation $\sigma_{\mathbf{X}_{lp}}$ of the lowpass filtered image $\mathbf{X}_{lp}$, the threshold value can be set adaptively for each image as $\mathcal{T}_U = c \cdot \sigma_{\mathbf{X}_{lp}}$. The larger the value of c, the more areas are considered to be uniform. The value of c is empirically set to 0.03.

2) CALCULATE REFERENCE DETAIL AMOUNT

We employed the guided filter [27] (GF) to measure the detail amount. The GF decomposes an input image $\mathbf{X}$ into two parts as follows:

$$\mathbf{X}(p) = \mathbf{B}(p) + \mathbf{D}(p), \tag{16}$$

where $\mathbf{B}$ is a base layer formed by homogeneous regions with sharp edges, $\mathbf{D}$ is a detail layer which contains noise or textures, and p is a pixel location in an image, i.e., $p = (i, j)$. The GF yields an edge-preserving smoothing output $\mathbf{B} = f_{\text{GF}}(\mathbf{X}, \mathbf{G}; s, \epsilon)$ of an input image $\mathbf{X}$ by considering the content of a guidance image $\mathbf{G}$ as

$$\mathbf{B}(p) = a_{p'}\mathbf{G}(p) + b_{p'}, \forall p \in \mathcal{W}_s(p'), \tag{17}$$

where $\mathcal{W}_s(p')$ is a square window centered at pixel p' with a size s. $a_{p'}$ and $b_{p'}$ are constants in the window $\mathcal{W}_s(p')$ which

are obtained by minimizing a cost function $E(a_{p'}, b_{p'})$ [27]

$$E = \sum_{p \in \mathcal{W}_s(p')} \left[(a_{p'}\mathbf{G}(p) + b_{p'} - \mathbf{X}(p))^2 + \epsilon a_{p'}^2 \right], \quad (18)$$

where ϵ is a regularization parameter that controls the amount of smoothing in the output image. We empirically set $s = 5 \times 5$ and $\epsilon = (0.1 \times 255)^2$.

The guided filter output $\mathbf{X}_{\mathrm{GF}}$ is calculated by using the original image $\mathbf{X}$ and itself as the guidance image as $\mathbf{X}_{\mathrm{GF}} = f_{\mathrm{GF}}(\mathbf{X}, \mathbf{X})$. A detail layer in uniform regions of the original image $\widetilde{\mathbf{D}}_X$ is calculated as:

$$\widetilde{\mathbf{D}}_X(p) = |\mathbf{X}(p) - \mathbf{X}_{\mathrm{GF}}(p)| \cdot \mathbf{U}(p) \cdot (\mathbf{X}(p)/\kappa), \quad (19)$$

where $\kappa = 255$ is a weighting coefficient. Then, the reference detail amount in the uniform regions of the original image is calculated as

$$\mathcal{D}_X = \frac{1}{N} \sum_{p=1}^{N} \widetilde{\mathbf{D}}_X(p), \quad (20)$$

where N is the total number of pixels in the image, i.e., $N = H \times W$.

3) CALCULATE OVER-CONTRAST MEASURE

A detail layer in uniform regions of the processed image $\widetilde{\mathbf{D}}_Y$ is calculated as

$$\widetilde{\mathbf{D}}_Y(p) = |\mathbf{Y}(p) - \mathbf{Y}_{GF}(p)| \cdot \mathbf{U}(p) \cdot (\mathbf{X}(p)/\kappa), \quad (21)$$

where $\mathbf{Y}_{\mathrm{GF}} = f_{\mathrm{GF}}(\mathbf{Y}, \mathbf{X})$. Note that we use the original image $\mathbf{X}$ as the guidance image to precisely estimate the amplified detail amount in $\mathbf{Y}$.[5] The detail amount of the processed image $\mathcal{D}_Y$ is calculated as

$$\mathcal{D}_Y = \frac{1}{N} \sum_{p=1}^{N} \widetilde{\mathbf{D}}_Y(p). \quad (22)$$

Finally, the over-contrast measure (OCM) is calculated as

$$\mathrm{OCM} = \mathcal{D}_Y - \mathcal{D}_X. \quad (23)$$

The value of OCM is usually positive in a contrast-enhanced image, and it has a negative value when noise is suppressed in uniform regions of the processed image with respect to the original image.

To our best knowledge, this is the first time to deal with the limitation of the performance of IQA metrics for contrast-changed images. Hence, there are no open datasets to evaluate the performance of the proposed metric. Therefore, to test the performance of OCM, we inspected the correlation between OCM and our viewing experience. The calculated OCM values in all datasets [28]–[31] are listed in Table 1. The results show that OCM is well consistent with our viewing experience. For example, HE and CLAHE often produce excessively amplified noise in uniform regions, so their OCM values are high in every dataset. For a more direct example,

[5]We also use $\mathbf{X}(p)/\kappa$ as the weighting factor in (21) to accurately estimate the amplified detail amount in $\mathbf{Y}$ with respect to $\mathbf{X}$.

FIGURE 10. Detected uniform regions of (a) *Hats*, (b) *Headlight*, and (c) *Market*.

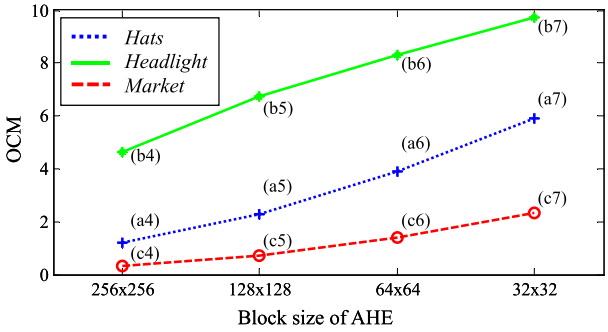

FIGURE 11. OCM measures of Fig. 8(a4)-(a7), (b4)-(b7), and (c4)-(c7) with respect to the original images in Fig. 8(a0)-(c0).

we calculated OCM values for the overly contrasted images generated by changing block sizes of AHE in Fig. 8. Detected uniform regions of the three images are shown in Fig. 10. As the block size decreases, the amount of contrast increase, accordingly corresponding OCM values increase proportionally as shown in Fig. 11. It is also well correlated with the actual viewing experience.

V. EXPERIMENTAL RESULTS

A. EXPERIMENTAL SETUP

1) TESTING DATASETS

To evaluate our proposed algorithms, we used five datasets of *CSIQ* [28], *TID2013* [29], *CCID2014* [30], *BSDS* [31]. The *CSIQ* image dataset contains 116 images which are generated by altering contrast at different levels with respect to 30 reference images. *TID2013* contains 24 types of subsets generated from 25 reference images considering various kinds of distortions. We used 250 images from contrast-changed and intensity shifted subsets. *CCID2014* contains 655 images which come from the original 15 images by contrast-alteration. *BSDS* contains 500 natural images from a wide range of contents such as humans, animals, indoor, outdoor and underwater scenes.

2) ALGORITHMS

The proposed RDST and RDAST algorithms were compared with ten CE Algorithms: HE [9], WTHE [10], HMF [12], AGCWD [11], SMIR [22], COTH [19], ROHIM [15], BOIEM [16], RDHM [13] (sorted in published order), and CLAHE [24]. CLAHE and RDAST are local CE methods where the block size is set to $\lfloor W/8 \rfloor \times \lfloor H/8 \rfloor$. In CLAHE, the clip limit was set to $0.01 \times MN$. Parameters of the

TABLE 1. Quantitative assessment of CE algorithms using six metrics. High scores mean high performance except that OCM is the opposite. Boldfaced fonts represent top two results among global algorithms. Each arrow represents relative performance from the lowest to the highest: ⇓ < ↓ < ↘ < → < ↗ < ↑ < ⇑.

	Global									Local	
Metrics	HE [9]	WTHE [10]	HMF [12]	AGCWD [11]	SMIR [22]	COTH [19]	ROHIM [15]	BOIEM [16]	RDHM [13]	RDST	CLAHE [24]	RD AST
CSIQ [28] (#116)												
DE	→ 6.278	↗ **6.374**	↗ 6.362	↓ 5.938	↗ 6.366	↘ 6.178	↘ 6.159	↑ **6.632**	→ 6.310	→ 6.297	⇑ 7.482	⇑ 7.692
PixDist	↑ 41.347	↑ 39.327	↘ 29.888	↓ 24.261	↑ **41.651**	↑ 41.634	↗ 37.003	↓ 25.317	↑ 40.993	↑ **42.404**	↘ 31.159	↑ 40.452
EMEG	↑ **0.242**	↗ 0.205	↘ 0.155	↓ 0.129	↗ 0.218	↑ 0.223	↗ 0.204	↓ 0.126	↑ 0.228	↑ **0.233**	↑ 0.222	↗ 0.209
QRCM	↑ 0.239	↑ 0.258	→ 0.172	↓ 0.040	↑ **0.275**	↑ 0.261	↗ 0.214	↓ 0.080	↑ 0.257	↑ **0.263**	⇑ 0.294	↑ 0.265
CPCQI	↗ 1.097	↑ **1.161**	↗ 1.120	↓ 0.960	↑ **1.157**	↑ 1.134	↘ 1.015	→ 1.048	↑ 1.136	↑ 1.149	⇑ 1.249	↑ 1.137
OCM	↓ 0.438	→ 0.236	↑ 0.104	↑ **0.032**	↗ 0.180	→ 0.224	↗ 0.114	↑ **0.102**	↘ 0.333	↘ 0.307	↓ 0.396	↗ 0.123
TID2013 [29] (#250)												
DE	↘ 6.645	→ **6.781**	→ **6.781**	↓ 6.517	→ 6.776	→ 6.758	↓ 6.511	↑ **7.097**	↘ 6.714	↘ 6.698	⇑ 7.517	⇑ 7.587
PixDist	↑ **43.078**	↗ 39.468	↓ 33.568	↓ 33.722	↗ 40.447	→ 38.326	→ 37.974	↓ 31.534	↑ 41.557	↑ **42.762**	↘ 34.774	↗ 40.367
EMEG	↑ **0.275**	→ 0.241	↓ 0.205	↘ 0.216	↗ 0.249	→ 0.235	→ 0.236	↓ 0.193	↑ 0.260	↑ **0.269**	⇑ 0.293	↑ 0.260
QRCM	↗ 0.144	↑ 0.156	↘ 0.096	↓ 0.071	↑ **0.167**	↗ 0.148	↘ 0.103	↓ 0.064	↑ 0.158	↑ **0.173**	⇑ 0.237	⇑ 0.189
CPCQI	↗ 1.070	↑ **1.104**	↗ 1.073	↓ 0.980	↑ **1.104**	↑ 1.094	↓ 1.000	→ 1.042	↑ 1.094	↑ **1.105**	⇑ 1.226	⇑ 1.105
OCM	↓ 0.348	↗ 0.168	↑ 0.103	↑ 0.086	↗ 0.133	↗ 0.134	↑ **0.082**	↑ **0.075**	↘ 0.254	→ 0.219	⇓ 0.460	↑ 0.121
CCID2014 [30] (#655)												
DE	↘ 6.430	→ **6.539**	→ 6.535	↓ 6.255	→ 6.531	→ 6.490	↘ 6.374	↑ **6.746**	→ 6.483	→ 6.465	⇑ 7.352	⇑ 7.551
PixDist	↑ **41.958**	↗ 38.940	↘ 32.833	↘ 33.997	↑ 39.984	↗ 37.631	↗ 38.219	↓ 29.931	↑ 40.640	↑ **42.407**	↘ 34.417	↑ 40.510
EMEG	↑ **0.277**	↗ 0.244	↓ 0.206	→ 0.227	↗ 0.252	→ 0.236	↗ 0.244	↓ 0.192	↑ 0.260	↑ **0.273**	⇑ 0.286	↑ 0.262
QRCM	→ 0.128	↑ 0.157	→ 0.109	↓ 0.076	↑ **0.174**	↗ 0.145	→ 0.117	↓ 0.060	↑ 0.154	↑ **0.170**	⇑ 0.235	⇑ 0.186
CPCQI	↘ 1.005	↑ 1.070	↑ 1.069	↓ 0.982	↑ **1.086**	↑ 1.064	↓ 0.967	→ 1.022	↗ 1.046	↑ **1.074**	⇑ 1.194	↑ 1.075
OCM	↓ 0.474	↗ 0.199	↑ 0.112	↑ 0.126	↗ 0.143	↗ 0.145	↑ **0.097**	↑ **0.051**	↘ 0.314	→ 0.231	↓ 0.402	↑ 0.108
BSDS [31] (#500)												
DE	→ 6.986	↗ 7.129	↗ **7.130**	↓ 6.811	↗ 7.101	↗ 7.118	↓ 6.763	↑ **7.255**	→ 7.042	→ 7.023	⇑ 7.663	⇑ 7.739
PixDist	↑ **42.693**	→ 39.214	↓ 35.472	→ 38.103	↗ 41.064	→ 37.889	↑ **42.707**	↓ 34.616	↑ 41.342	↑ 42.515	↘ 36.335	↗ 40.550
EMEG	↑ **0.260**	↘ 0.219	↓ 0.198	→ 0.222	→ 0.233	↘ 0.210	↑ **0.253**	↓ 0.194	↗ 0.242	↑ 0.248	⇑ 0.288	↑ 0.247
QRCM	→ 0.094	↗ 0.107	↘ 0.074	↓ 0.067	↑ **0.128**	→ 0.097	→ 0.093	↓ 0.057	↗ 0.110	↑ **0.121**	⇑ 0.215	⇑ 0.153
CPCQI	↗ 1.052	↑ **1.082**	↑ 1.063	↓ 0.967	↑ **1.084**	↑ 1.073	↘ 0.995	→ 1.035	↑ 1.075	↑ **1.082**	⇑ 1.209	⇑ 1.105
OCM	↓ 0.505	↗ 0.161	↑ 0.091	↑ **0.056**	↑ 0.094	↑ 0.097	↑ **0.035**	↑ **0.035**	→ 0.316	↗ 0.197	↓ 0.465	↑ 0.126
Average (#1521)												
DE	↘ 6.636	↗ **6.760**	→ 6.758	↓ 6.457	→ 6.746	→ 6.717	↓ 6.508	↑ **6.962**	→ 6.692	→ 6.674	⇑ 7.491	⇑ 7.629
PixDist	↑ **42.337**	↗ 39.146	↓ 33.597	↘ 34.559	↑ 40.542	↗ 38.135	↗ 39.561	↓ 31.382	↑ 41.048	↑ **42.501**	↘ 34.858	↑ 40.495
EMEG	↑ **0.268**	→ 0.232	↓ 0.199	↘ 0.216	↗ 0.243	→ 0.226	↗ 0.243	↓ 0.188	↗ 0.252	↑ **0.261**	⇑ 0.283	↑ 0.253
QRCM	↗ 0.128	↑ 0.148	↘ 0.100	↓ 0.069	↑ **0.165**	↗ 0.138	→ 0.114	↓ 0.061	↑ 0.148	↑ **0.161**	⇑ 0.233	⇑ 0.181
CPCQI	→ 1.038	↑ 1.086	↑ 1.072	↓ 0.975	↑ **1.094**	↑ 1.077	↓ 0.985	→ 1.031	↑ 1.071	↑ **1.087**	⇑ 1.208	⇑ 1.094
OCM	↓ 0.460	↗ 0.184	↑ 0.103	↑ 0.089	↑ 0.128	↑ 0.133	↑ **0.075**	↑ **0.054**	↘ 0.306	→ 0.224	↓ 0.432	↑ 0.117

others were set as recommended in the corresponding papers. Color images were converted from RGB to HSV color space. CE methods were only applied to value components, and then inverse color space transformation was performed to reconstruct contrast-enhanced images in the RGB color space.

B. QUANTITATIVE ASSESSMENT

To evaluate the quantitative performance of algorithms, we used six IQA metrics. Discrete entropy (DE) [33], pixel distance (PixDist) [34], and expected measure of enhancement by the gradient (EMEG) [20] were used as no-reference metrics. Quality-aware relative contrast measure (QRCM) [22], a color considered patch-based contrast quality index (CPCQI) [16], and our proposed over-contrast measure (OCM) were used as full-reference metrics.

The objective assessment results of the twelve algorithms are shown in Table 1, where high scores denote high performance for all metrics except that OCM is the opposite, and the best and the second-best performance among global algorithms are highlighted in bold. For each row, the score of jth algorithm $\mathcal{S}_j$ was normalized to calculate relative performance as

$$\hat{\mathcal{S}}_j = \frac{\mathcal{S}_j - \min\mathcal{S}_G}{\max\mathcal{S}_G - \min\mathcal{S}_G}, \tag{24}$$

where $\max\mathcal{S}_G$ and $\min\mathcal{S}_G$ represent the maximum and the minimum scores of the global CE algorithms, respectively. The arrows next to each score indicate the relative performance calculated as $\Downarrow = \{\hat{\mathcal{S}}_j | \hat{\mathcal{S}}_j < 0\}$, $\downarrow = \{\hat{\mathcal{S}}_j | 0 \le \hat{\mathcal{S}}_j \le 0.2\}$, $\searrow = \{\hat{\mathcal{S}}_j | 0.2 < \hat{\mathcal{S}}_j \le 0.4\}$, $\rightarrow = \{\hat{\mathcal{S}}_j | 0.4 < \hat{\mathcal{S}}_j \le 0.6\}$, $\nearrow = \{\hat{\mathcal{S}}_j | 0.6 < \hat{\mathcal{S}}_j \le 0.8\}$, $\uparrow = \{\hat{\mathcal{S}}_j | 0.8 < \hat{\mathcal{S}}_j \le 1\}$, and

$\Uparrow = \{\hat{\mathcal{S}}_j | \hat{\mathcal{S}}_j > 1\}$. In the case of OCM, the reverse range was applied so that $\Uparrow$ always represents the best performance. Due to the issue mentioned at Section IV-A, the current IQA metrics tend to give high scores to overly contrasted images. Therefore, with the help of the OCM, we evaluate each CE algorithms more accurately as follows:

1) THE AMOUNT OF INFORMATION

In Shannon's information theory, discrete entropy (DE) is a measure for the amount of information in an image as

$$\mathcal{S}_{\mathrm{DE}} = -\sum_{k} p(k) \log\, p(k), \tag{25}$$

where $p(k)$ is the probability distribution at the kth gray-level. A high DE indicates that the image contains more variations and conveys more information. RDAST attained the highest value of DE in all datasets as shown in Table 1. It means that the resulting images of RDAST contain more information than the results of the other methods.

2) DYNAMIC RANGE UTILIZATION

Pixel distance (PixDist) calculates the average gray-level difference overall pixel pairs in an image as [34]

$$\mathcal{S}_{\mathrm{PixDist}} = \frac{1}{N(N-1)} \sum_{k=1}^{K} \sum_{k'=k}^{K} p(k) p(k') (k' - k), \tag{26}$$

where $k, k' \in [0, K]$, N is the total number of pixels in $\mathbf{X}$. A high value of PixDist means histogram components are uniformly distributed without concentrating at particular gray-levels. Therefore, HE shows high performance of PixDist. However, it has the lowest performance of OCM. On the other hand, RDST not only has the best performance of PixDist but also has better performance of OCM as shown in Table 1. It means that the RDST makes the best use of the given dynamic range while suppressing noise amplification in uniform regions. RDAST also has excellent performance of dynamic range utilization.

3) DIRECT CONTRAST MEASURE

The expected measure of enhancement by gradient (EMEG) is defined as [20]

$$\mathcal{S}_{\mathrm{EMEG}} = \frac{1}{B} \sum_{b=1}^{B} \frac{1}{\kappa} \max\left(\frac{\max \mathbf{X}_{dx}^{b}}{\min \mathbf{X}_{dx}^{b}}, \frac{\max \mathbf{X}_{dy}^{b}}{\min \mathbf{X}_{dy}^{b}} \right), \tag{27}$$

where $\mathbf{X}_{dx}^{b}$ and $\mathbf{X}_{dy}^{b}$ are the absolute-valued derivatives in x and y direction of bth block, respectively. B is the total number of blocks, and $\kappa = 255$ is a weighting coefficient.[6] A high value of EMEG means that an enhanced image has high contrast which we expect as a result of CE. Although CLAHE achieves the highest performance of EMEG, its OCM performance is low due to amplified noise in homogeneous regions. In contrast, the proposed RDAST has good performance of OCM as well as high performance of EMEG as shown in Table 1. In addition, RDST has excellent performance of contrast improvement in terms of EMEG.

4) QUALITY-AWARE RELATIVE CONTRAST MEASURE (QRCM)

QRCM [22] is a function of relative contrast measure (RCM) and gradient magnitude similarity map (GMS) [38] as

$$\mathcal{S}_{\mathrm{QRCM}} = f(\mathrm{RCM}, \mathrm{GMS}). \tag{28}$$

It employed GMS to quantify the level of distortions. Therefore, QRCM[7] provides not only measure the relative change of contrast but also considers the distortion introduced on the processed image relative to the original image. This ability seems to work well within global algorithms, but not in local algorithms since the QRCM value of CLAHE is approximately 1.5 times higher on average than the highest QRCM value in global algorithms. Among global algorithms, RDST shows the excellent performance of QRCM. Except for the contrast over-stretching CLAHE algorithm, the proposed RDAST provides the best performance in terms of QRCM as shown in Table 1.

5) THE LATEST HIGH-PERFORMANCE IQA METRIC

A patch-based contrast quality index (PCQI) [35] has been proven to be highly correlated with subjective quality scores in contrast-changed datasets. Colorfulness-based PCQI (CPCQI) is the extended version of PCQI that takes into account the influence of colorfulness as [16]

$$\mathcal{S}_{\mathrm{CPCQI}} = \frac{1}{N} \sum_{i=1}^{N} \mathbf{q}_{\mathrm{mi}}(i) \cdot \mathbf{q}_{\mathrm{cc}}(i) \cdot \mathbf{q}_{\mathrm{sd}}(i) \cdot \mathbf{q}_{\mathrm{cs}}(i), \tag{29}$$

where $\mathbf{q}_{\mathrm{mi}}$, $\mathbf{q}_{\mathrm{cc}}$, $\mathbf{q}_{\mathrm{sd}}$, and $\mathbf{q}_{\mathrm{cs}}$, respectively, represent the similarity between the original and processed images in terms of mean intensity, contrast change, structural distortion, and color saturation. Although CLAHE attains the highest value of CPCQI, it has low performance of OCM. Except for the CLAHE, the RDAST shows the best performance of CPCQI. RDST also shows excellent performance in terms of CPCQI among the global algorithms as shown in Table 1.

In summary, the proposed RDAST shows the best or superior performance in every metric. RDST also has excellent performance. Although it does not have the best performance of OCM, it does not generate noticeable artifacts as shown in Figs. 12–17. This fact is also supported by our viewing experience for all datasets.

C. QUALITATIVE ASSESSMENT

A qualitative analysis was performed on the resulting images produced by applying the CE methods for selected images from each dataset. The first test image is *Cactus* from the *CSIQ* dataset [28] which has a small contrast degradation with respect to the pristine image. The CE results with the

[6] When implementing EMEG, a small constant should be added to each denominator in (27) to prevent division by zero [20]. $\mathcal{S}_{\mathrm{EMEG}} \in [0, 1]$.

[7] $\mathcal{S}_{\mathrm{QRCM}} \in [-1, 1]$, where -1 and 1 refer to the full levels of contrast degradation and improvement, respectively.

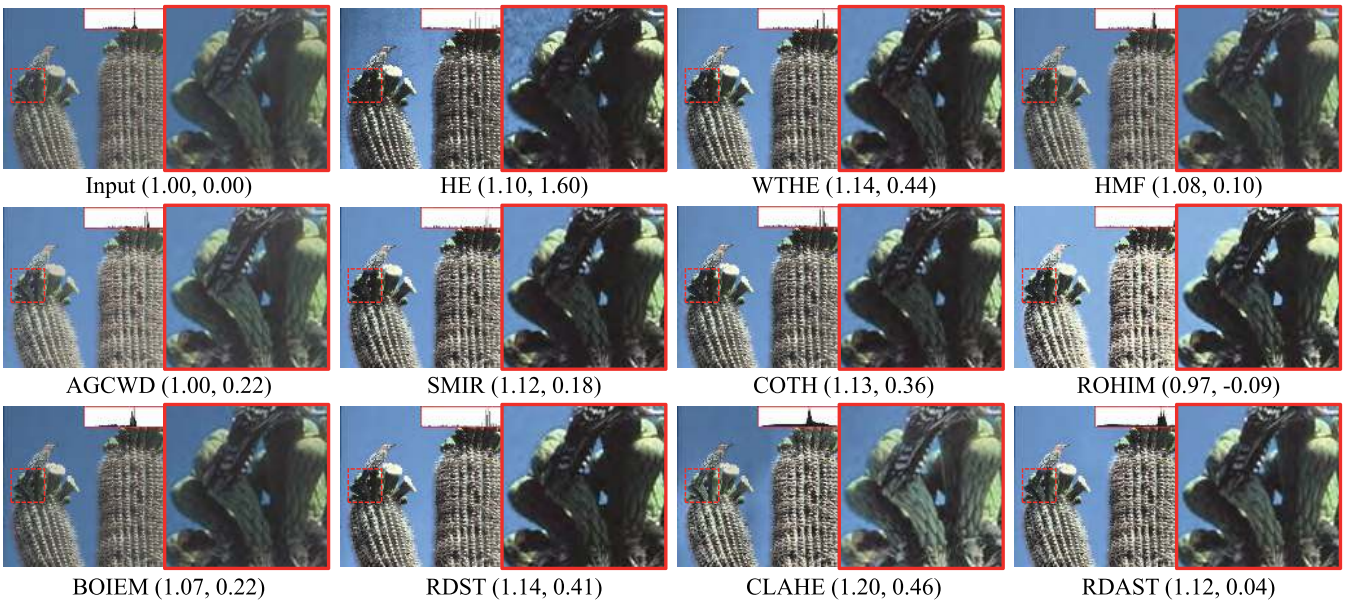

FIGURE 12. Comparisons of CE results on *Cactus* image [28]. Corresponding CPCQI and OCM values are in parenthesis. Some remarkable regions are enlarged.

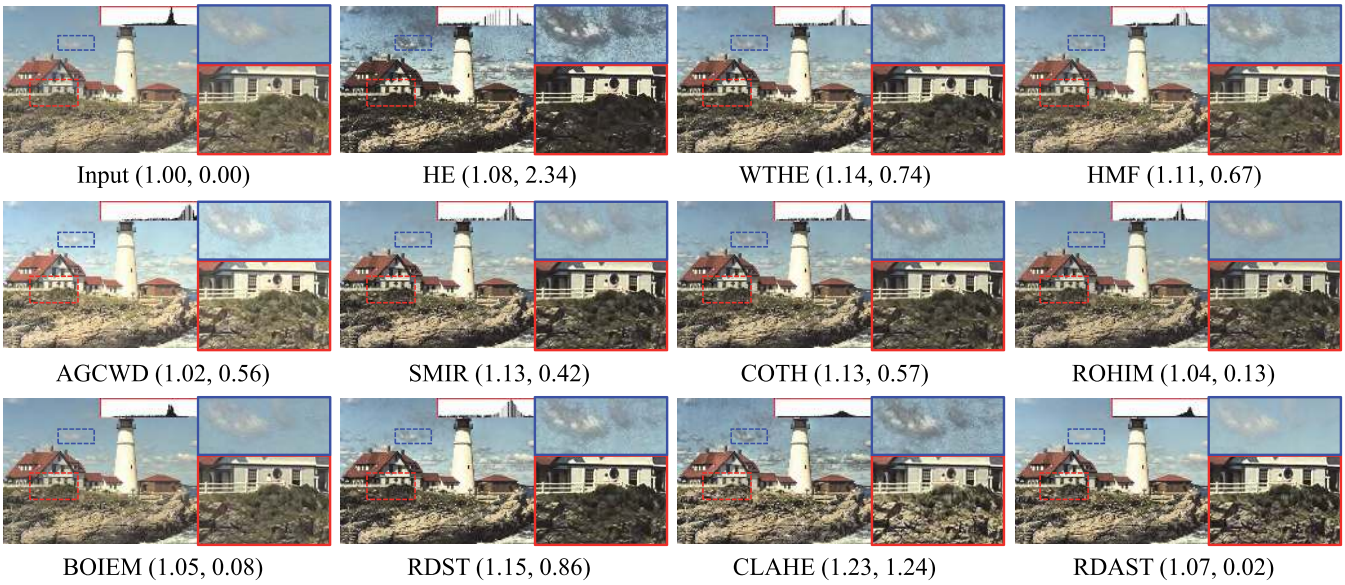

FIGURE 13. Comparisons of CE results on *Headlight* image [29]. Corresponding CPCQI and OCM values are in parenthesis. Some remarkable regions are enlarged with colored rectangles.

corresponding CPCQI and OCM values (in parenthesis), histograms, and enlarged images are shown in Fig. 12. It has a uniform background which corresponds to the highest peak in the input histogram. HE tries to spread out the highest peak in the input histogram. As a result, the noise in the background was excessively amplified, and significant under-enhancement occurred around the stem of the flowers. Although CLAHE generated a detail improved image, it has noticeable noise amplification in the background with halo artifacts. HMF, AGCWD, ROHIM, and BOIEM produced slightly contrast altered images. It is supported by the CPCQI values around 1. WTHE, SMIR, COTH, RDST, and RDAST achieved significant contrast improvements in overall quality. Among these methods, however, only RDAST generated the detail enhanced image with suppressed noise in the background. It is also supported by the high CPCQI value and the low OCM value.

The second image *Headlight* [29] and its enhancement results are shown in Fig. 13. The input image was generated by adding a constant value to all pixels of the pristine image. Therefore, there is a margin at the far left of the input histogram that can be used to improve the contrast

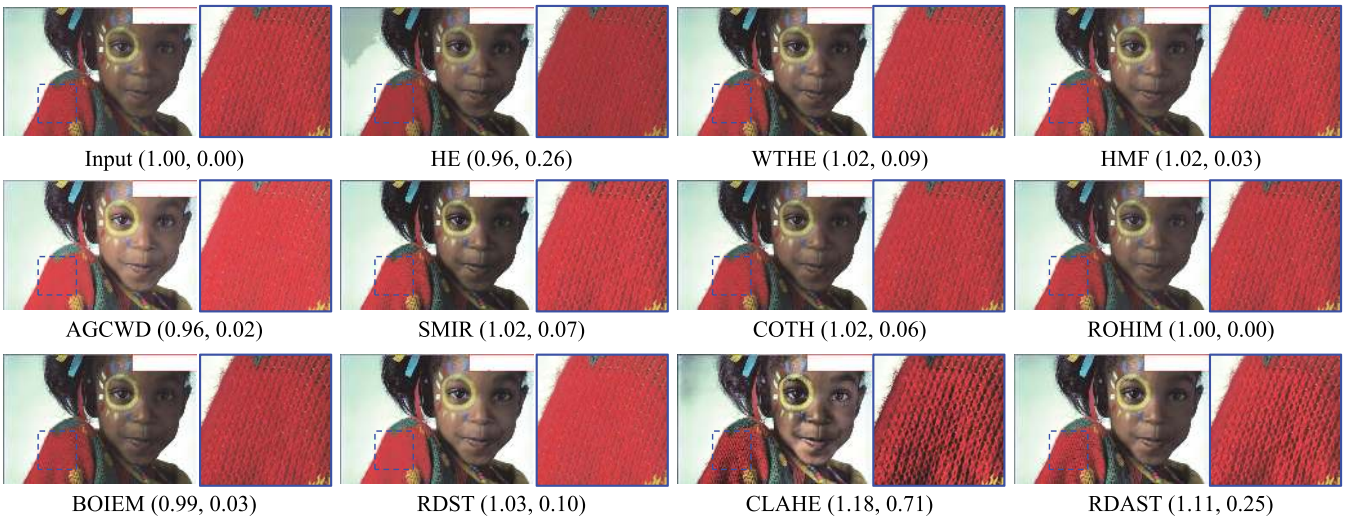

FIGURE 14. Comparisons of CE results on *Girl* image [30]. Corresponding CPCQI and OCM values are in parenthesis. Some remarkable regions are enlarged.

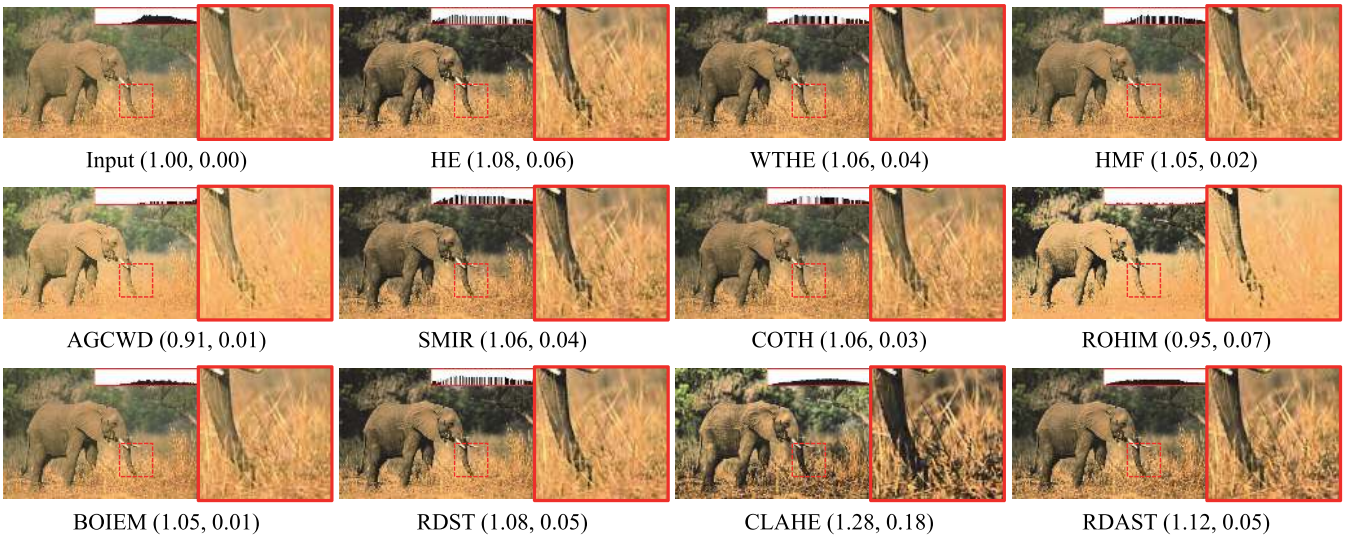

FIGURE 15. Comparisons of CE results on *Elephant* image [31]. Corresponding CPCQI and OCM values are in parenthesis. Some remarkable regions are enlarged.

further. However, HMF, AGCWD, ROHIM, and BOIEM did not fully exploit the entire dynamic range. Although HE and CLAHE fully utilized the whole dynamic range, they created overly enhanced images with excessively amplified noise in the sky. WTHE, SMIR, COTH, and RDST achieved contrast enhancement, but noise in the sky also increased. However, RDAST achieved significant contrast improvements while effectively enhancing textured regions and suppressing noise amplification in uniform regions.

The third image *Girl* [30] is shown in Fig. 14. It has the highest peak at the rightmost side of the input histogram, which corresponds to the background. HE produced artifacts in the background. CLAHE produced excessively amplified noise in the background with blocking artifacts on the face. Among the global algorithms, RDST produced an image with adequate brightness and contrast. The resulting image of RDAST significantly improved the texture of the red shirt and had no visual artifacts on the face and the backgrounds.

The fourth image *Elephant* [31] is shown in Fig. 15. It is a slightly blurred image with a margin on the left side of the input histogram. AGCWD produced an excessively bright image with markedly degraded contrast. The resulting image of ROHIM contains visual artifacts with missing details. CLAHE produced a severely distorted image with halo artifacts and checkerboard effects. Among the other methods, RDST and RDAST produced a more vivid image with a natural look.

Next, Fig. 16 shows *Flower* images [28] and the corresponding enhancement results. Input images provide different levels of global contrast decrement from no global

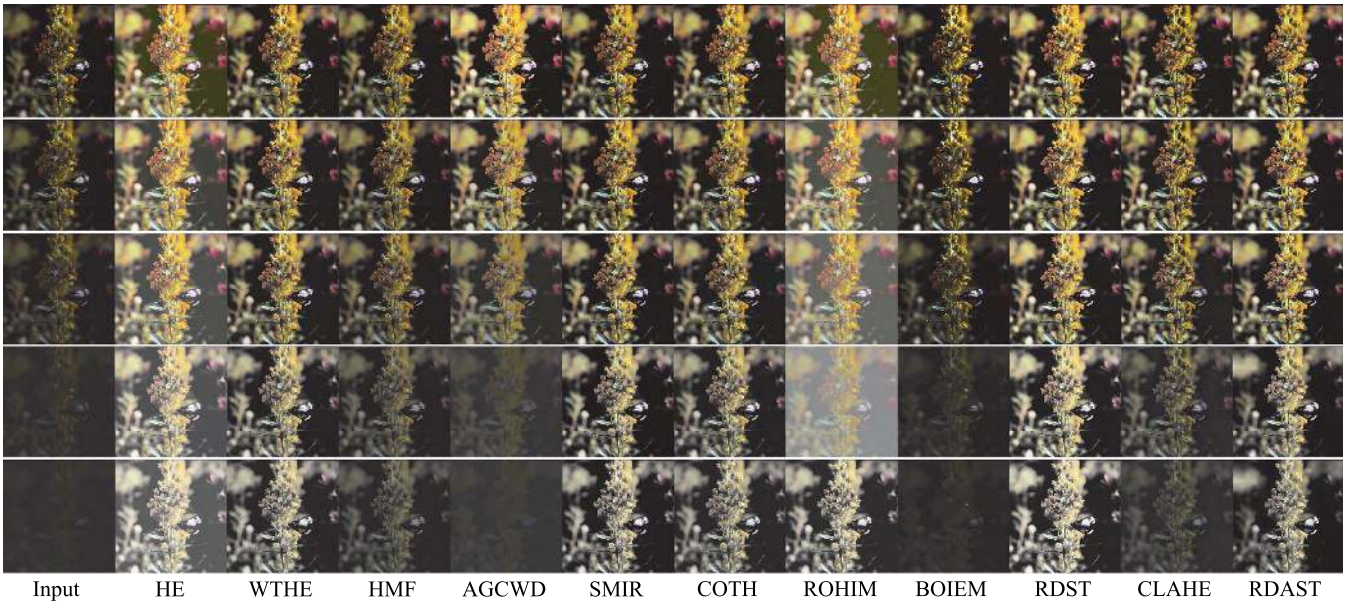

FIGURE 16. Contrast enhancement results on *Flower* images [28] with different levels of contrast decrement.

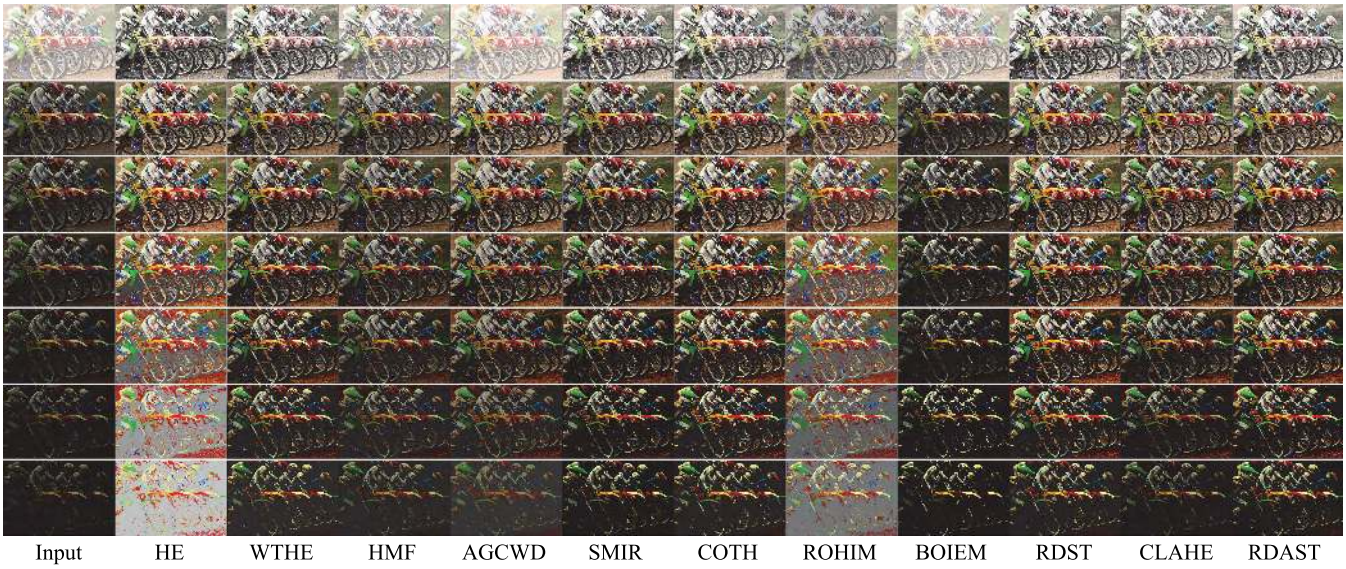

FIGURE 17. Comparisons of CE results on *Bikes* image [30] with different levels of brightness decrement. (File names: "img110.png" – "img116.png").

contrast decrement (row 1) to severe contrast decrement (row 5). Therefore, It is suitable images for evaluating the CE capability of each algorithm in contrast-degraded images. HE and ROHIM produced noticeably distorted images because the background gray-levels were not mapped appropriately. HMF, AGCWD, BOIEM, and CLAHE generated unsatisfactory images as the contrast of the input image decreased. Among the other methods, RDST and RDAST improved the contrast satisfactorily even at the severely contrast-degraded input images.

Finally, Fig. 17 shows *Bikes* images [30], where the brightness of input images is further decreased from the first row to the last row. Therefore, they are suitable to evaluate the contrast improvement capability of each CE algorithm in various brightness conditions. Both HE and ROHIM produced very serious luminance and color distortion. AGCWD also generated an inappropriate luminance image at the last row of the figure. The contrast enhancement capability of HMF and BOIEM is not satisfactory. However, RDAST and RDST consistently produce good quality images.

We also performed the popular paired comparison as a subjective quality assessment test for 192 images (16 original images and associated 176 images generated by eleven CE algorithms) of Figs. 12–17. Twenty subjects consisting of 15 males and 5 females participated in the test. The subjects were asked to select an image of higher quality between a

TABLE 2. Subjective assessment scores of the input and each of contrast-enhanced images. Top two results are boldfaced.

Image	Input	HE	WTHE	HMF	AGCWD	SMIR	COTH	ROHIM	BOIEM	RDST	CLAHE	RDAST
Cactus	54	2	115	143	91	**175**	133	94	78	173	61	**201**
Headlight	155	2	58	86	105	114	108	166	**175**	118	39	**194**
Girl	58	27	123	153	125	112	137	121	98	**173**	14	**179**
Elephant	53	150	151	117	27	173	134	16	90	**174**	57	**178**
Flower-row1	59	21	163	113	82	160	147	25	62	**185**	120	**183**
Flower-row2	43	33	156	91	68	145	139	16	78	**190**	170	**191**
Flower-row3	41	55	168	96	39	173	150	13	67	**191**	128	**199**
Flower-row4	42	101	165	85	25	180	160	20	43	**189**	108	**202**
Flower-row5	23	84	155	85	7	**181**	175	133	30	178	80	**189**
Bikes-row1	25	149	154	77	9	167	142	86	39	**189**	112	**171**
Bikes-row2	21	167	108	57	112	152	134	83	17	**182**	110	**177**
Bikes-row3	25	106	108	66	132	152	173	42	20	**185**	127	**184**
Bikes-row4	45	30	143	92	102	142	185	5	45	**200**	140	**191**
Bikes-row5	45	5	161	93	103	141	183	18	53	**195**	126	**197**
Bikes-row6	49	1	165	114	91	150	172	19	57	**205**	106	**191**
Bikes-row7	68	2	144	99	47	165	167	19	96	**198**	115	**200**
Average	50	58	140	98	73	155	152	55	66	**183**	101	**189**

TABLE 3. Comparisons of calculation times with standard deviations on different size of images. (* Indicates implementation with MEX functions).

	Average Calculation Times (ms)		
Algorithms	768×512	1920×1080	3840×2160
*HE	4 ± 1	10 ± 1	40 ± 3
*WTHE	4 ± 1	11 ± 0	41 ± 3
*HMF	4 ± 1	11 ± 1	43 ± 4
*AGCWD	4 ± 1	10 ± 1	42 ± 2
SMIR	565 ± 100	2,384 ± 248	8,928 ± 729
COTH	148 ± 25	409 ± 21	1,484 ± 54
ROHIM	8,174 ± 4,338	40,666 ± 9,505	157,532 ± 30,479
BOIEM	2,146 ± 46	5,538 ± 119	18,117 ± 524
*RDST	4 ± 1	12 ± 1	43 ± 2
*CLAHE	17 ± 3	54 ± 2	150 ± 6
*RDAST	31 ± 4	107 ± 4	342 ± 16

pair of images of the same scene corresponding to different conditions. The elaborately designed software shortened the evaluation time by scoring through simple manipulations that select a better image by pressing the right or left arrow key. We tabulated the vote counts, i. e., the number of times one image was selected as better than any other images, in Table 2. Note that the higher the score, the better the performance. The average subjective rating scores indicate that the proposed RDST and RDAST have highly competitive performance.

D. CALCULATION TIME

To provide calculation times for different size of images, we chose CCID2014 dataset [30] which consists of 644 images of 768×512 size. We resized the images to 1280×720, 1920×1080 (Full HD), and 3840×2160 (4K image). The average calculation times for each algorithm are shown in Table 3. All algorithms were implemented in MATLAB R2014a. The algorithms which were implemented using MEX functions to calculate an input histogram and the mapping function between input and output gray-levels are denoted by the asterisk (*) in Table 3. Tests were performed on a personal computer running 64-bit Windows 7 with 16.0 GB RAM and Intel Core i7-4940 MX 3.3 GHz CPU. As the size of the input images increases, the processing time for SMIR, ROHIM, and BOIEM increases dramatically. However, the processing time of the others, including the proposed algorithms, increase in proportion to the image size. The proposed RDST algorithm is one of the fastest algorithms with high performance. The processing time of the RDAST is much faster than SMIR, and it provides the best CE performance as shown in Table 1 and 2.

VI. CONCLUSION

We have introduced the use of ramp distribution as an NSS model for CE and proposed two CE algorithms. A ramp distribution-based slant thresholding (RDST) algorithm is proposed as a global CE method. It employs a slant thresholding technique to improve the contrast effectively. A ramp distribution-based adaptive slant thresholding (RDAST) algorithm is also proposed as a local CE method. It adaptively adjusts a slant angle of the ramp distribution in each block to avoid noise amplification in uniform regions and to maximize contrast in non-uniform regions. RDAST also employs a scaled global modified histogram to minimize the effect of block size changes on the resulting image. The parameters used in RDAST are designed to be automatically adjusted. Besides, it can achieve a fairly consistent quality image for various block size settings.

In order to measure the over-contrast amount with respect to a reference image, an over-contrast measure is introduced. The metric is based on the characteristics of the human visual system that amplified noise in uniform regions is more distinctive than non-uniform regions. So, the OCM uses a local standard deviation map to detect uniform regions and

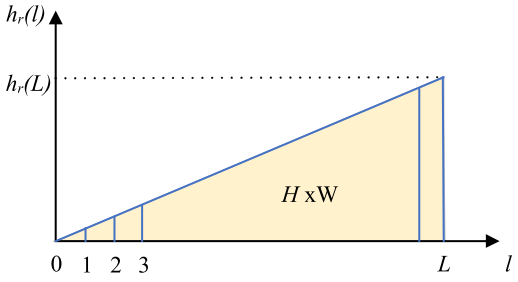

FIGURE 18. Illustration of a ramp-distributed histogram $\mathbf{H}_r$.

employs the guided filter to measure the amount of details in uniform regions.

Quantitative and qualitative experimental tests have been performed on a wide range of images. With the help of the OCM, we were able to correctly evaluate all CE algorithms including local CE algorithms. Our proposed algorithms produce better or comparable contrast-enhanced images than state-of-the-art algorithms. Due to its simplicity and computational efficiency, the proposed RDST and RDAST can be easily applied to a wide range of real-world applications.[8]

APPENDIX
PROOF OF EQUATION (2)

The total sum of $\mathbf{H}_r$ is equal to the area of the triangle in a discrete domain as shown in Fig. 18. Let us divide the triangle equally into L, then the total sum of division equals to $H \times W$. Therefore, $HW = \frac{1}{2}(L+1) \times h_r(L)$, then $h_r(L) = \frac{2HW}{L+1}$. Note that the base length of the triangle is $L+1$ because it is calculated in the discrete domain. Since $h_r(l)$ is directly proportional to l, we can obtain the proportional expression as $l : h_r(l) = L : h_r(L)$. Therefore,

$$h_r(l) = h_r(L)\frac{l}{L} = \frac{2HW}{L+1} \times \frac{l}{L} = \frac{2HW}{L(L+1)}l. \qquad (30)$$

REFERENCES

[1] T. Ayyavoo and J. J. Suseela, "Illumination pre-processing method for face recognition using 2D DWT and CLAHE," *IET Biometrics*, vol. 7, no. 4, pp. 380–390, Jul. 2018.
[2] A. F. M. Raffei, H. Asmuni, R. Hassan, and R. M. Othman, "A low lighting or contrast ratio visible iris recognition using iso-contrast limited adaptive histogram equalization," *Knowl., Based Syst.*, vol. 74, pp. 40–48, Jan. 2015.
[3] A. Fabija ska, "Automatic segmentation of corneal endothelial cells from microscopy images," *Biomed. Signal Process. Control*, vol. 47, pp. 145–158, Jan. 2019.
[4] S. Sajeev, M. Bajger, and G. Lee, "Segmentation of breast masses in local dense background using adaptive clip limit-CLAHE," in *Proc. Int. Conf. Digit. Image Comput., Techn. Appl. (DICTA)*, Nov. 2015, pp. 1–8.
[5] Sonali, S. Sahu, A. K. Singh, S. P. Ghrera, and M. Elhoseny, "An approach for de-noising and contrast enhancement of retinal fundus image using CLAHE," *Opt. Laser Technol.*, vol. 110, pp. 87–98, Feb. 2018.
[6] J. Joseph, J. Sivaraman, R. Periyasamy, and V. R. Simi, "An objective method to identify optimum clip-limit and histogram specification of contrast limited adaptive histogram equalization for MR images," *Biocybern. Biomed. Eng.*, vol. 37, no. 3, pp. 489–497, 2017.

[8]MATLAB code will be released at http://cilabs.kaist.ac.kr/Publication/international-journal

[7] Z. Sinno, C. Caramanis, and A. C. Bovik, "Towards a closed form second-order natural scene statistics model," *IEEE Trans. Image Process.*, vol. 27, no. 7, pp. 3194–3209, Jul. 2018.
[8] J. Xiao, J. Hays, K. A. Ehinger, A. Oliva, and A. Torralba, "SUN database: Large-scale scene recognition from abbey to zoo," in *Proc. IEEE Comput. Soc. Conf. Comput. Vis. Pattern Recognit.*, Jun. 2010, pp. 3485–3492.
[9] R. C. Gonzalez and R. E. Woods, *Digital Image Processing*, 3rd ed. Englewood Cliffs, NJ, USA: Prentice-Hall, 2007.
[10] Q. Wang and R. K. Tan, "Fast image/video contrast enhancement based on weighted thresholded histogram equalization," *IEEE Trans. Consum. Electron.*, vol. 53, no. 2, pp. 757–764, May 2007.
[11] S.-C. Huang, F.-C. Cheng, and Y.-S. Chiu, "Efficient contrast enhancement using adaptive gamma correction with weighting distribution," *IEEE Trans. Image Process.*, vol. 22, no. 3, pp. 1032–1041, Mar. 2013.
[12] T. Arici, S. Dikbas, and Y. Altunbasak, "A histogram modification framework and its application for image contrast enhancement," *IEEE Trans. Image Process.*, vol. 18, no. 9, pp. 1921–1935, Sep. 2009.
[13] S. Lee, D. Kim, and C. Kim, "Ramp distribution-based image enhancement techniques for infrared images," *IEEE Signal Process. Lett.*, vol. 25, no. 7, pp. 931–935, Jul. 2018.
[14] K. Gu, G. Zhai, X. Yang, W. Zhang, and C. W. Chen, "Automatic contrast enhancement technology with saliency preservation," *IEEE Trans. Circuits Syst. Video Technol.*, vol. 25, no. 9, pp. 1480–1494, Sep. 2015.
[15] K. Gu, G. Zhai, W. Lin, and M. Liu, "The analysis of image contrast: From quality assessment to automatic enhancement," *IEEE Trans. Cybern.*, vol. 46, no. 1, pp. 284–297, Jan. 2016.
[16] K. Gu, D. Tao, J.-F. Qiao, and W. Lin, "Learning a no-reference quality assessment model of enhanced images with big data," *IEEE Trans. Neural Netw. Learn. Syst.*, vol. 29, no. 4, pp. 1301–1313, Apr. 2018.
[17] T. Celik and T. Tjahjadi, "Contextual and variational contrast enhancement," *IEEE Trans. Image Process.*, vol. 20, no. 12, pp. 3431–3441, Dec. 2011.
[18] C. Lee, C. Lee, and C.-S. Kim, "Contrast enhancement based on layered difference representation of 2D histograms," *IEEE Trans. Image Process.*, vol. 22, no. 12, pp. 5372–5384, Dec. 2013.
[19] D. Kim and C. Kim, "Contrast enhancement using combined 1-D and 2-D histogram-based techniques," *IEEE Signal Process. Lett.*, vol. 24, no. 6, pp. 804–808, Jun. 2017.
[20] T. Celik, "Spatial entropy-based global and local image contrast enhancement," *IEEE Trans. Image Process.*, vol. 23, no. 12, pp. 5298–5308, Dec. 2014.
[21] T. Celik and L. Heng-Chao, "Residual spatial entropy-based image contrast enhancement and gradient-based relative contrast measurement," *J. Mod. Opt.*, vol. 63, no. 16, pp. 1600–1617, 2016.
[22] T. Celik, "Spatial mutual information and pagerank-based contrast enhancement and quality-aware relative contrast measure," *IEEE Trans. Image Process.*, vol. 25, no. 10, pp. 4719–4728, Oct. 2016.
[23] S. M. Pizer, E. P. Amburn, J. D. Austin, R. Cromartie, A. Geselowitz, T. Greer, B. T. H. Romeny, and J. B. Zimmerman, "Adaptive histogram equalization and its variations," *Comput. Vis., Graph., Image Process.*, vol. 39, no. 3, pp. 355–368, 1987.
[24] A. M. Reza, "Realization of the contrast limited adaptive histogram equalization (CLAHE) for real-time image enhancement," *J. VLSI Signal Process. Syst. Signal, Image Video Technol.*, vol. 38, no. 1, pp. 35–44, 2004.
[25] Y. Chang, C. Jung, P. Ke, H. Song, and J. Hwang, "Automatic contrast-limited adaptive histogram equalization with dual gamma correction," *IEEE Access*, vol. 6, pp. 11782–11792, 2018.
[26] V. E. Vickers, "Plateau equalization algorithm for real-time display of high-quality infrared imagery," *Opt. Eng.*, vol. 35, pp. 1921–1926, Jul. 1996.
[27] K. He, J. Sun, and X. Tang, "Guided image filtering," *IEEE Trans. Pattern Anal. Mach. Intell.*, vol. 35, no. 6, pp. 1397–1409, Jun. 2013.
[28] E. C. Larson and D. M. Chandler, "Most apparent distortion: Full-reference image quality assessment and the role of strategy," *J. Electron. Imag.*, vol. 19, no. 1, pp. 011006-1–011006-21, Mar. 2010.
[29] N. Ponomarenko, L. Jin, O. Ieremeiev, V. Lukin, K. Egiazarian, J. Astola, B. Vozel, K. Chehdi, M. Carli, F. Battisti, and C.-C. J. Kuo, "Image database TID2013: Peculiarities, results and perspectives," *Signal Process., Image Commun.*, vol. 30, pp. 57–77, Jan. 2015.
[30] *Contrast-Changed Image Database 2014*. Accessed: Jun. 2019. [Online]. Available: https://sites.google.com/site/guke198701/publications
[31] P. Arbeláez, M. Maire, C. Fowlkes, and J. Malik, "Contour detection and hierarchical image segmentation," *IEEE Trans. Pattern Anal. Mach. Intell.*, vol. 33, no. 5, pp. 898–916, May 2011.

[32] K. A. Panetta, E. J. Wharton, and S. S. Agaian, "Human visual system-based image enhancement and logarithmic contrast measure," *IEEE Trans. Syst., Man, Cybern. B, Cybern.*, vol. 38, no. 1, pp. 174–188, Feb. 2008.
[33] C. E. Shannon, "A mathematical theory of communication," *Bell Syst. Tech. J.*, vol. 27, no. 4, pp. 623–656, Oct. 1948.
[34] Z. Chen, B. R. Abidi, D. L. Page, and M. A. Abidi, "Gray-level grouping (GLG): An automatic method for optimized image contrast Enhancement—Part I: The basic method," *IEEE Trans. Image Process.*, vol. 15, no. 8, pp. 2290–2302, Aug. 2006.
[35] S. Wang, K. Ma, H. Yeganeh, Z. Wang, and W. Lin, "A patch-structure representation method for quality assessment of contrast changed images," *IEEE Signal Process. Lett.*, vol. 22, no. 12, pp. 2387–2390, Dec. 2015.
[36] M. A. Saad, P. Le Callet, and P. Corriveau, "Blind image quality assessment: Unanswered questions and future directions in the light of consumers needs," *VQEG E-Lett.*, vol. 1, no. 2, pp. 62–66, Dec. 2014. [Online]. Available: ftp://vqeg.its.bldrdoc.gov/eLetter/Issues/VQEG_eLetter_vol01_issue2.pdf
[37] L. Krasula, K. Fliegel, P. L. Callet, and M. Klíma, "Quality assessment of sharpened images: Challenges, methodology, and objective metrics," *IEEE Trans. Image Process.*, vol. 26, no. 3, pp. 1496–1508, May 2017.
[38] W. Xue, L. Zhang, X. Mou, and A. C. Bovik, "Gradient magnitude similarity deviation: A highly efficient perceptual image quality index," *IEEE Trans. Image Process.*, vol. 23, no. 2, pp. 684–695, Feb. 2014.
[39] S. Wolf, "Measuring the end-to-end performance of digital video systems," *IEEE Trans. Broadcast.*, vol. 43, no. 3, pp. 320–328, Sep. 1997.
[40] H. Yu and S. Winkler, "Image complexity and spatial information," in *Proc. IEEE Int. Workshop Qual. Multimedia Exper. (QoMEX)*, Jul. 2013, pp. 12–17.
[41] E. Peli, "Contrast in complex images," *J. Opt. Soc. Amer. A, Opt. Image Sci.*, vol. 7, no. 10, pp. 2032–2040, Oct. 1990.

SEUNGYOUN LEE received the B.S. degree *(summa cum laude)* in electronics engineering and education and the M.S. degree in electronics engineering from Chungnam National University, Daejeon, South Korea, in 2003 and 2005, respectively. He has been a Senior Researcher with the Agency for Defense Development, Daejeon, South Korea, since 2005. He has authored or coauthored more than 20 papers in journals and conferences and holds more than seven patents. His research interests include image enhancement, infrared image processing, video coding, wireless video transmission, and embedded system design.

CHANGICK KIM (SM'09) received the B.S. degree in electrical engineering from Yonsei University, Seoul, South Korea, in 1989, the M.S. degree in electronics and electrical engineering from the Pohang University of Science and Technology, Pohang, South Korea, in 1991, and the Ph.D. degree in electrical engineering from the University of Washington, Seattle, WA, USA, in 2000. From 2000 to 2005, he was a Senior Member of Technical Staff with Epson Research and Development, Inc., Palo Alto, CA, USA. From 2005 to 2009, he was an Associate Professor with the School of Engineering, Information and Communications University, Daejeon, South Korea. Since 2009, he has been with the School of Electrical Engineering, Korea Advanced Institute of Science and Technology (KAIST), Daejeon, Korea, where he is currently a Professor. His research interests include multimedia signal processing and computer vision.